THE JOURNAL OF PHYSICAL CHEMISTRY C
A JOURNAL OF THE AMERICAN CHEMICAL SOCIETY

pubs.acs.org/JPCC

Article

Nonlinear Magnetic Field Dependence of Quantum Beats in $FAPbI_3$

Isaac Brown,[#] Rikard Bodin,[#] Uyen Huynh, Peter C. Sercel, Stephen McGill, Dmitry Semenov, and Zeev Valy Vardeny*

Cite This: *J. Phys. Chem. C* 2025, 129, 5973−5979

Read Online

ACCESS | Metrics & More | Article Recommendations | Supporting Information

ABSTRACT: We present evidence for the magnetic field dependence of the electron and hole Landé g-factors in films of the hybrid organic−inorganic perovskite formamidinium lead iodide $HC(NH_2)_2PbI_3$ (FAPI). We perform transient pump−probe Kerr spectroscopy on FAPI in magnetic fields up to 25 T, which reveals a significant deviation from the expected linear dependence of the quantum beating frequency on the applied magnetic field. We also found a decrease of the quantum beating frequencies with increasing pump intensity for a fixed magnetic field. These observations are discussed in terms of the dependence of the electron and hole Landé *g*-factors on the band gap, within a simple model in which the effective band gap increases at high magnetic field due to Landau level formation and increases with increasing pump intensity by virtue of shifts in the quasi-Fermi levels.

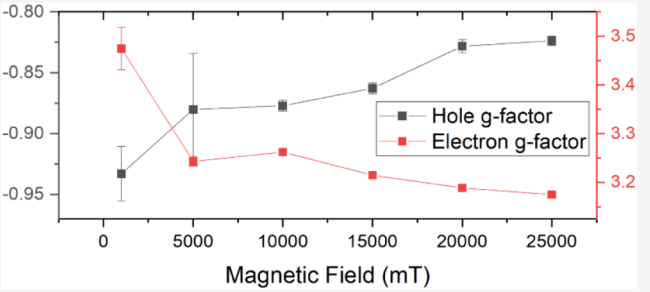

1. INTRODUCTION

Many variations on the hybrid organic−inorganic perovskite have been explored in recent years, due to promising optoelectronic properties such as a wide range of bandgap tunability[1] and interesting spin dynamics. Previous studies into methylammonium lead iodide (MAPI) perovskite have revealed long spin lifetimes[2−4] (∼10 ns) in addition to the strong spin−orbit coupling effects due to the presence of lead, making such materials quite intriguing for applications in spin quantum computation. Based on the Kerr resonances measured in the S.I. (Figure S3) showing several zero-crossings, the perovskite $HC(NH_2)_2PbI_3$ ($FAPbI_3$ or FAPI) possesses a bandgap of 1.51 eV at a temperature of 12 K in our thin films. This places it just outside the visible spectrum, making this material potentially more interesting than MAPI for solar cell applications.[5] Both compounds can be produced using notably inexpensive spin-casting techniques. These materials have inspired considerable research into solar cells, owing to the swift advancement of their efficiency over the past decade. FAPI has a perovskite crystal structure, characterized as ABX_3, where the A-site is occupied by a cation, the B-site is the heavy atom, and the X-site is occupied by a halide. There is a structural phase transition from cubic to the beta-tetragonal phase at 285 K and another transition at 140 K, between the beta phase and gamma phase of the tetragonal structure.[6,7] Our measurements are done at 12 K, putting us in the gamma-tetragonal phase.

Time-resolved Faraday rotation (TRFR) has been a very useful technique for investigating spin dynamics in direct band gap semiconductors, in both crystals and films.[8−10] In the present work, we used TRFR spectroscopy on neat FAPI films, using degenerate pump and probe, from a single pulsed Ti-Sapphire laser, with a typical spectral width of 5 nm at FWHM. Quantum beats in films of $CsPbBr_3$ have been measured up to high magnetic fields (B < 60 T),[11] where the exciton Zeeman splitting energy was shown to be linear in the applied magnetic field over the full range from 0 to 60 T. Here, we report our investigation of the magnetic field dependence of electron and hole Landé g-factors in films of FAPI. Our investigations show that the electron and hole Landé g-factors in FAPI films exhibit a nonlinear dependence on magnetic field when tested at high magnetic fields up to 25 T. Effects due to the intensity of the optical pump have also been investigated previously in other systems, but no changes to the measured quantum beating frequency have previously been observed, although changes to the photoexcitation relaxation rate are known.[12] In this work, we report pump-intensity dependence of the measured carrier g-factors in FAPI films. We explain these results in terms of pump dependence of the quasi-Fermi energies leading to significant deviations of the observed g-factor due to carrier density and magnetic field.

Received: December 6, 2024
Revised: February 23, 2025
Accepted: March 7, 2025
Published: March 18, 2025

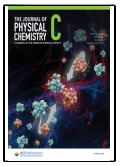

https://doi.org/10.1021/acs.jpcc.4c08269
J. Phys. Chem. C 2025, 129, 5973−5979

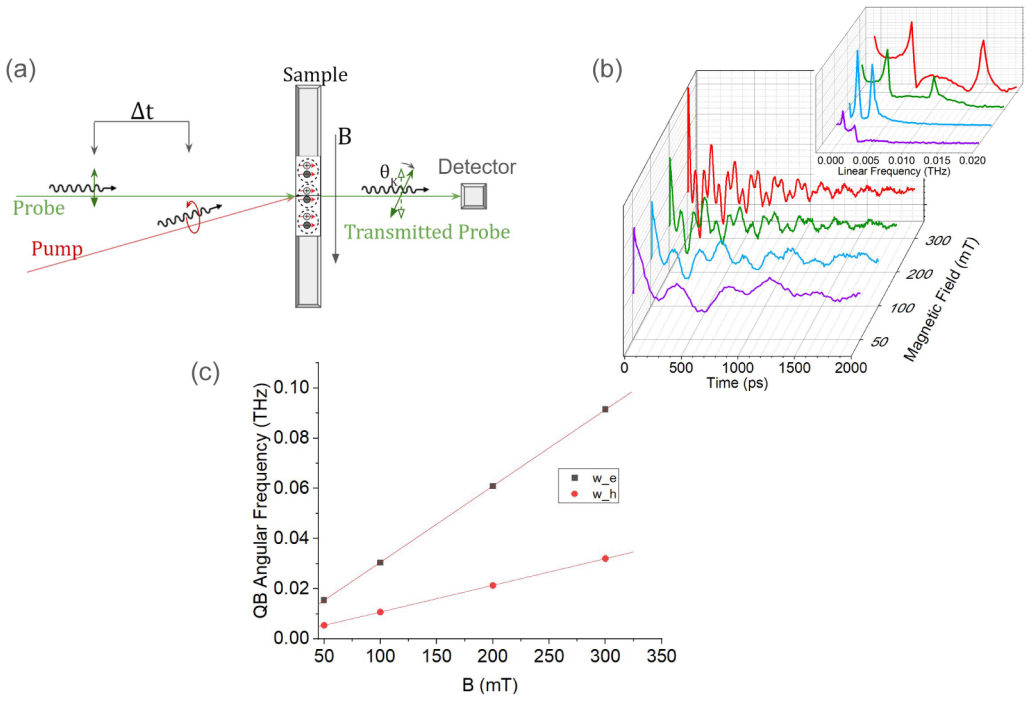

Figure 1. Quantum beats from FAPI at relatively low field along with the associated FFT. (a) The time-resolved Faraday rotation setup with a magnetic field oriented in the Voigt configuration (see the text). (b) The TRKR response in a FAPI film at various magnetic fields; the inset shows the related FFT spectra. Two clear quantum beat frequencies are observed. (c) The transient quantum beat angular frequencies ω from Figure 1b vs the applied magnetic field. The fit straight line gives the respective Lande' g-factor of holes gh = 1.25 and electron ge = 3.63, for magnetic fields $B \leq 300$ mT.

2. METHODS

Our primary experiments have been done using TRFR on thin films, with which we measure the transient quantum beating (QB) signal of the optically excited spin carriers in FAPI. In Figure 1a, we show the TRFR setup, with pump and probe pulses separated by a time delay Δt. The pump beam is circularly polarized, and the probe beam is linearly polarized. In the measurement, the polarization angle of the probe light changes due to the influence of the pump-beam. A magnetic field is applied in the Voigt geometry (in-plane to the sample), and the rotation of the probe's polarization axis is measured by a balanced photodiode bridge. For our TRFR setup, we use a degenerate pump−probe scheme using a Ti-Sapphire pulsed laser having a repetition rate of 76 MHz. Our closed-loop He cryostat cools the sample to 12 K, where we measure the TRFR signal at various pump excitation intensities and temperatures. The pulses of the Ti-Sapphire laser are separated by ∼12.5 ns, which gives a large time interval for observing QBs, which are resolved on the order of hundreds to thousands of picoseconds (see Figure 1b). Typically, at relatively low pump intensities, the photogenerated spin lifetime in FAPI is significantly smaller than the pulse separation time of 12.5 ns,[1] but if FAPI is analogous to other hybrid perovskites in terms of the spin physics, we would expect the spin lifetime of a high-quality single crystal to be much longer. Other efforts have measured spin relaxation lifetimes of >10 ns in single-crystal MAPI,[13] which can lead to a spin resonance amplification effect. However, for our deposited films, the lifetimes are closer to 1 ns with a narrow laser bandwidth of 5 nm fwhm. When pumped with a laser energy of 843 nm at zero magnetic field, FAPI produces a clean biexponential decay. The lifetimes were measured to be τ_h = 1.2 ns and τ_e = 100 ps at 12 K. With an applied magnetic field, we observe distinct quantum beats, shown in Figure 1b. The high magnetic field data were measured at the National High Magnetic Field Laboratory, or MagLab, in Tallahassee Florida. When measured at the facility at MagLab, the pulsed laser was centered at 820 nm, having a broader bandwidth of 30 nm fwhm. Here, a lifetime of roughly 20 ps was observed due to various geometric and spectroscopic constraints, which we explore in the Supporting Information. We were able to reconcile the two data sets using measurements at B = 1 T, but only after normalizing the low-field data according to the observed pump intensity dependence.

3. RESULTS AND DISCUSSION

As seen in Figure 1, the QB contains two oscillations with fast and slow frequencies. These responses can be fit using a linear combination of damped harmonic oscillators of the form

$$\text{TRFR} = A_1 e^{-t/t_1}\cos\omega_1 t + A_2 e^{-t/t_2}\cos\omega_2 t \quad (1)$$

where t_1 and t_2 are the measured T_2* lifetimes of each QB component. The decoherence lifetimes show dependences on pump intensity, temperature, and magnetic field, which are explored in the (see Figures S1 and S4 and the discussion of these figures in the Supporting Information Experimental Section). However, the bulk of this work is focused on the QB frequencies. In the FAPI film, there are two distinct QB signals—the electron at high QB frequency, and the hole at a lower QB frequency.[1] Alternatively, we could assign them to a positive trion at high QB frequency and negative trion at lower QB frequency[13] since the g-values of positive (negative) trions are the same as those of the electron (hole); also, some studies suggest that the photoexcitations could be excitonic in MAPI.

https://doi.org/10.1021/acs.jpcc.4c08269
J. Phys. Chem. C 2025, 129, 5973−5979

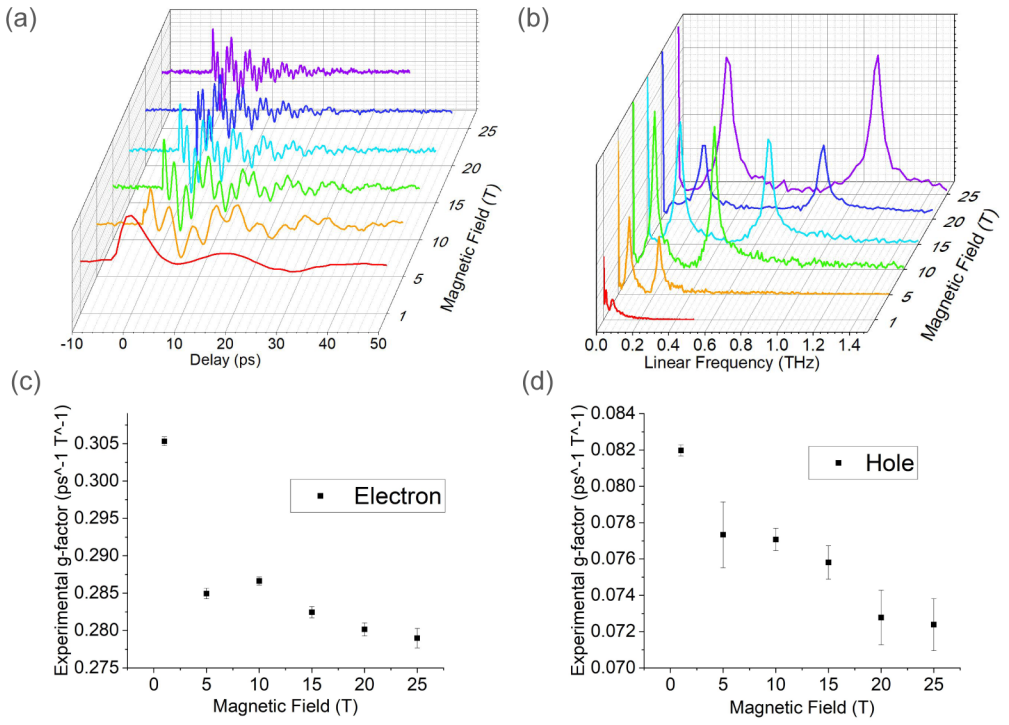

Figure 2. Quantum beat response from FAPI film at various fields in the high-B regime (a), along with the associated FFT (b). (c) and (d) the obtained experimental g-factors, $g_{ex} = \omega/B$ at each magnetic field for electrons and holes, respectively.

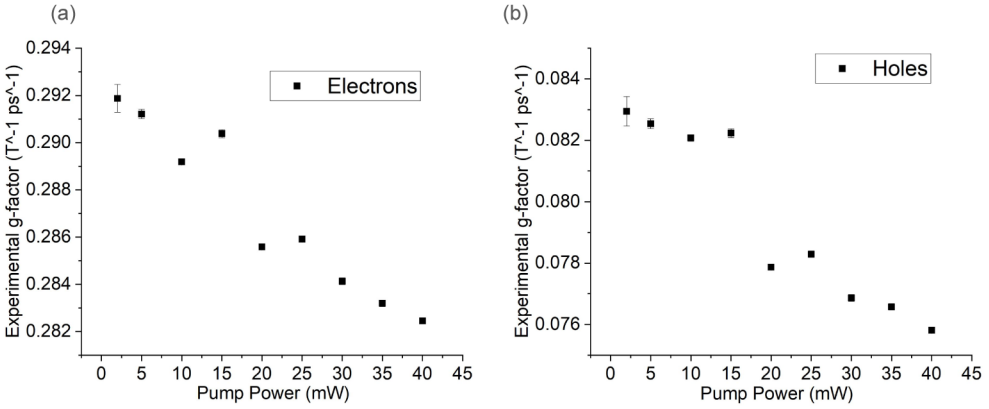

Figure 3. Power dependence of the "experimental g-factor", $g_{exp} = \omega/B$ for the electrons (a) and holes (b), respectively. The downward trend indicates that an increased excitation density introduces changes to the quasi-Fermi level, which, in turn decreases g_{exp}.

Ultimately, it is difficult to say exactly what the spin species are in this experiment.[14−17] In the inset of Figure 1b, we see the associated Fourier transforms, showing the two clear QB frequencies at each magnetic field, from which we may estimate the error bar involved in the beating frequencies.

In Figure 1c, we show the quantum beat frequencies as a function of the applied magnetic field. This type of plot is typically shown to extract the Lande' g-factor, which assumes that the quantum beat frequencies are linear with magnetic field, according to Larmor precession, given in eq 2,

$$\omega_L = g\mu_B B/\hbar \tag{2}$$

where g is the electron/hole Lande' g-factor, μ_B is the Bohr magneton, B is the applied magnetic field, and $\hbar$ is the reduced Planck's constant. This plot shows Lande' g-factors of $g_{h,ex}$ = 1.25 and $g_{e,ex}$ = 3.63, and the linear fit passes through what is essentially the origin, indicating a lack of significant influences on the spin Hamiltonian from terms lacking magnetic field dependence. In Figure 2, we see the same type of plot as in Figure 1b, but at much higher magnetic fields. These data were taken at MagLab. These high-field data show something unusual, which has not previously been reported in hybrid perovskites. When we use a plot of ω vs B to extract the "Lande' g-factor" at high field (see Supporting Information Text and Figure S3), we find electron and hole g-factors $g_{e,ex}$ = 3.21 and $g_{h,ex}$ = 0.84, which are significantly lower values for both species than were observed in the low-field data set, Figure 1c This is especially unusual since these measurements were performed on the same sample, although at different facilities. The discrepancy between the low-field and high-field data could have to do with sample degradation, but given the geometrical constraints of the two systems, we believe the difference can be explained by a small discrepancy in pump

https://doi.org/10.1021/acs.jpcc.4c08269
J. Phys. Chem. C 2025, 129, 5973−5979

intensity, which we will explain later during the discussion of the pump intensity dependence.

Attempts to fit the high-field Larmor frequency data to a linear dependence of ω vs B revealed unusual behavior in the fit residual. It appeared that there was a monotonic error as a function of the magnetic field. Attempts to explain this effect by introducing a nonmagnetic-field-dependent term in the spin Hamiltonian were unsuccessful, suggesting that this is not the proper explanation. So instead, we decided to plot a different quantity, which we call the "experimental g-factor", defined as the QB frequency divided by the applied field at each magnetic field point, $g_{exp}=\omega/B$. A plot of this quantity is shown in Figure 2c,d. These plots highlight the slight deviation from linearity of the g-value as a function of magnetic field, which cannot be explained by a frequency offset originating from possible magnetic-field-independent terms in the spin Hamiltonian. At high magnetic fields of B > 5 T, there is a monotonic decrease in the "experimental g-factor" that lies well outside of the error of our data, although it is small enough that it is difficult to see on a standard plot of ω vs B. Below we will show that this nonlinearity can be explained within a Landau level model. We suggest that the formation of Landau levels (LLs) at high magnetic fields has the effect of creating a magnetic-field-dependent increase in the band gap, which decreases the g factors At the same time, the quasi-Fermi energy shifts with increasing magnetic field as the density of states changes due to Landau level formation, also resulting in a monotonic decrease of both electron and hole g factors.

In Figure 3, we see the "experimental g-factors," $g_{exp}=\omega/B$ of electrons and holes as a function of pump intensity. Curiously, the magnitude of the g_{exp} decreases with increasing pump intensity, which has not been observed in similar measurements of other hybrid perovskites. The downward trend indicates that an increased excitation density introduces changes to the quasi-Fermi level, which in turn decrease the amplitude of the Lande' g-factor. These data were measured at 15 T. Curiously, the monotonic decrease of the experimental g-factor is well outside of error and provides an explanation for the g-factor discrepancy between our low-field data and our high-field data, which were measured using different cryostats and different laser systems. Due to the geometry of the experiment, we needed to use a higher pump intensity when measuring the data at Maglab to reach an acceptable level of signal-to-noise. This resulted in changes to the quasi-Fermi level of the excited population, lowering the g-factor. However, the observed magnetic field dependence must still be explained.

Using k.p theory, we show how certain assumptions can lead to a model that explains the magnetic field dependence in the Lande' g-factor that we observe at high magnetic fields. In Figure 4, we show a cartoon dispersion relation for a typical semiconductor, where the conduction band minimum (CBM) and valence band maximum (VBM) are separated by a bandgap energy E_g. For this case, with no magnetic field, the 3D DOS is as follows:

$$\mathrm{DOS}_{3d}(E) = \frac{1}{2\pi^2}\left(\frac{2m}{\hbar^2}\right)^{3/2} E^{1/2} \tag{3}$$

where m refers to the effective mass of carriers. When integrated, the carrier density scales as energy to the 3/2 power,

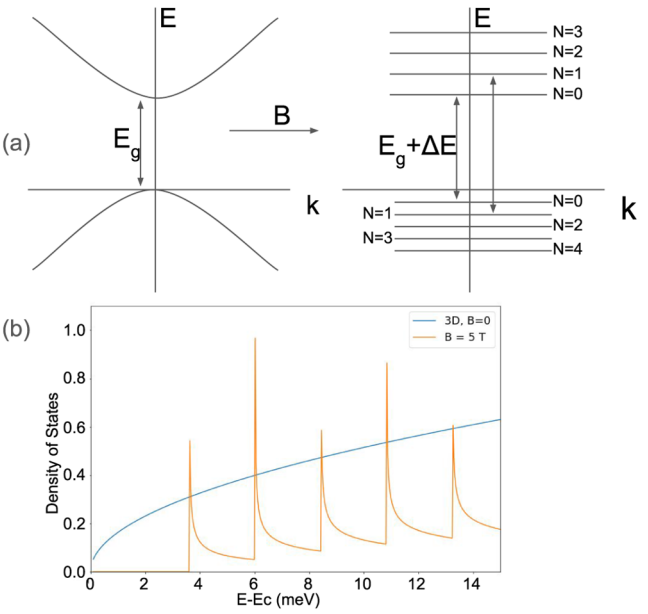

Figure 4. Quasi-Fermi level effects. (a) Magnetic field-induced conversion of the electron dispersion relation to one involving Landau levels (LLs). As the energy increases, new LLs become available, separated by discrete energy interval determined by the cyclotron frequency for each carrier. The density of states can be broken into two parts—the 2D DOS associated with the LLs in the plane perpendicular to the magnetic field and a magnetic field dependent DOS that accounts for the dispersion along the direction of the applied field, as described by eqs 3−7. (b) The density of states as a function of the quasi-Fermi energy that shows the onset energy of each Landau level at high field compared to the smooth density of states for the zero-field case.

$$N_{3d}(E) = \int_0^E \mathrm{DOS}_{3d}(E)dE = \frac{1}{3\pi^2}\left(\frac{2m}{\hbar^2}\right)^{3/2} E^{3/2} \tag{4}$$

At high magnetic fields, however, Landau levels (LLs) are formed. LLs are discrete energy levels associated with carrier motion in the plane perpendicular to the magnetic field, consisting of a discrete set of states separated by a uniform energy determined by the cyclotron frequency $\omega_c = \frac{qB}{m}$. Note that there are two separate populations here—a population of electrons, with $m = m_e$, and a population of holes, with $m = m_h$. Each Landau level has a degeneracy per unit area of $G = \frac{eB}{h}$ [18−22].

For motion in the direction parallel to the magnetic field, the carriers associated with a given Landau level, n, have a one-dimensional density of states function given by

$$\mathrm{DOS}_{1d}(E) = \frac{1}{\pi}\left(\frac{2m}{\hbar^2}\right)^{1/2}\left(E - \hbar\omega_c\left(n + \frac{1}{2}\right)\right)^{-1/2} \tag{5}$$

Therefore, the total B-dependent DOS apart from Zeeman splitting is as follows:

$$\mathrm{DOS}_B(E) = \frac{eB}{h}\sum_n \frac{1}{\pi}\left(\frac{2m}{\hbar^2}\right)^{1/2}\left(E - \hbar\omega_c\left(n + \frac{1}{2}\right)\right)^{-\frac{1}{2}} \tag{6}$$

where e is the charge of an electron and ω_c is the cyclotron frequency. Again, there is a separate cyclotron frequency for electrons and holes, and both populations are experiencing

https://doi.org/10.1021/acs.jpcc.4c08269
J. Phys. Chem. C 2025, 129, 5973−5979

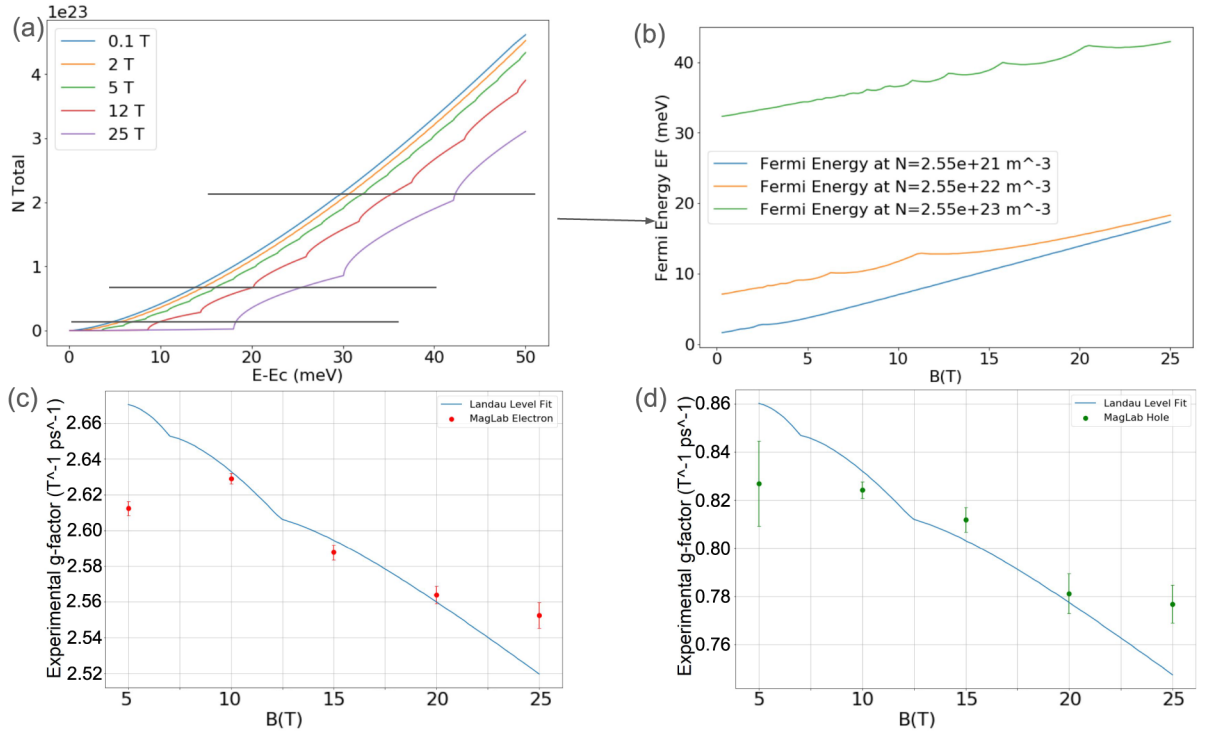

Figure 5. Electron and hole *g*-factor magnetic field effects from K·P theory. (a) The carriers' density as a function of the quasi-Fermi level, E_F, at various magnetic fields. (b) Parametric inversion of (a) showing the E_F as a function of the magnetic field for different excitation densities. (c, d) The best fit of the electron and hole Lande' g-factors calculated using the K·P model given in eqs 10 and 11.

these effects simultaneously. When integrated, the carrier density scales as the square root of the Landau level term $E - \hbar\omega_c(n + 1/2)$

$$N_B(E) = \int_0^E \mathrm{DOS}_B(E)dE = \frac{2eB}{\pi\hbar}\left(\frac{2m}{\hbar^2}\right)^{1/2} \sum_n \sqrt{E - \hbar\omega_c\left(n + \frac{1}{2}\right)} \tag{7}$$

Here, n represents the number of the Landau level in question. To fully calculate the magnetic-field-dependence, a sum must be taken over the number of Landau levels occupied. However, the effect of the Landau levels on the *g*-factor is periodic with the magnetic field, meaning that below a certain maximum magnetic field, adding more Landau levels has no effect on the field-dependent Lande' *g*-factor. Figure 5a shows the integrated carrier density as a function of Fermi energy, which is then inverted to produce Figure 5b, showing the Fermi energy as a function of magnetic field for certain constant carrier densities.

The expressions for the electron and hole g-factors have been explored previously, where a small external magnetic field is applied, and the resulting effective Zeeman Hamiltonian for the lowest conduction band and the valence band can be analyzed.[13] The resulting calculation gives an approximate *g*-factor expression for the cubic phase. We performed our measurements on a polycrystalline film, so it is not possible to measure the g-factor along two symmetry axes of the tetragonal phase, as one might do in a single crystal sample. Therefore, we use the cubic phase expression as an approximation. These expressions are

$$g_h^{\mathrm{cubic}} = g_0 - \frac{2}{3}E_p\left(\frac{1}{E_g} - \frac{1}{E_G + \Delta}\right) \tag{8}$$

$$g_e^{\mathrm{cubic}} = \frac{2}{3}\frac{E_p}{E_g} - (4\kappa_1 + 2) \tag{9}$$

These expressions must now be modified to account for the high magnetic field and high carrier density. In this regime, the effective band gap should reflect the transition between the greatest occupied LLs in the VB and CB, which will be reflected by the quasi-Fermi energy of both the valence band and conduction band. Therefore, the band gap shifts to $E_G + E_{FN} + E_{FP}$, where E_{FN} and E_{FP} are the conduction and valence band quasi-Fermi energies, respectively. In summary, the effect on the *g*-factor is described by eqs 10 and 11,

$$g_h^{\mathrm{cubic}} = g_0 - \frac{2}{3}E_p\left(\frac{1}{E_g + E_{FP} + E_{FN}} - \frac{1}{E_G + E_{FP} + E_{FN} + \Delta}\right) \tag{10}$$

$$g_e^{\mathrm{cubic}} = \frac{2}{3}\frac{E_p}{E_g + E_{FP} + E_{FN}} - (4\kappa_1 + 2) \tag{11}$$

In Figure 5c,d, we show the magnetic field dependences of the electron and hole Lande' *g*-factors as predicted by this model, together with a best fit using the LL model. Based on this model, we extract a carrier density of 3e22 m^{-3}, a Luttinger parameter of $\kappa = 0.225$, and a Kane energy of Ep = 13.7 eV, which closely match the values reported in other works.[13,23]

https://doi.org/10.1021/acs.jpcc.4c08269
J. Phys. Chem. C 2025, 129, 5973−5979

To synthesize the FAPI thin films, we created 1 M precursor solutions from 1 mol PbI_2 and 1 mol FAI powder, mixed with 1 mL of dimethylformamide (DMF) solvent. This solution was then left on a magnetic stirring plate for 24 h. We then spin-coated the solution onto glass substrates at 3000 rpm for 60 s and annealed them at 100 C for 1 hour. This process was done entirely within an inert nitrogen atmosphere.

4. CONCLUSIONS

In conclusion, the experimental g-factors of the photoexcited spin species in FAPI have a dependence on magnetic field and intensity at high magnetic fields. In the B > 5 T regime, the magnetic field dependence produces about a 10% deviation between 5 and 25 T. Since our trends show that the electron splitting will decrease with increased field and the negative hole splitting will decrease in magnitude, they will average out to something that appears constant with field. From 5 to 25 T, ω/B for the hole rises +0.006 ps^{-1} T^{-1}, and ω/B for the electron falls −0.006 ps^{-1} T^{-1}, averaging to zero between the two effects. Additionally, the pump intensity influences Lande' g-factor by about 5% over a 20-fold change in pump intensity. The intensity dependence can be explained by the shifting quasi-Fermi level due to carrier injection, which fills up the conduction band and shifts the effective band gap. The magnetic field dependence reflects a generation of Landau levels, as well as a field-dependent dispersion along the direction of the magnetic field. These effects have not been previously observed in other hybrid perovskites, even when measurements of quantum beats have been performed at high magnetic fields, such as in $CsPbBr_3$.

■ ASSOCIATED CONTENT

Supporting Information

The Supporting Information is available free of charge at https://pubs.acs.org/doi/10.1021/acs.jpcc.4c08269.

Photoluminescence, mechanical data, pictures of apparatus, and additional information (PDF)

■ AUTHOR INFORMATION

Corresponding Author

Zeev Valy Vardeny − *Department of Physics and Astronomy, University of Utah, Salt Lake City, Utah 84112, United States;* orcid.org/0000-0002-2298-398X; Email: val@physics.utah.edu

Authors

Isaac Brown − *Department of Physics and Astronomy, University of Utah, Salt Lake City, Utah 84112, United States;* orcid.org/0009-0002-3465-5577

Rikard Bodin − *Department of Physics and Astronomy, University of Utah, Salt Lake City, Utah 84112, United States*

Uyen Huynh − *Department of Physics and Astronomy, University of Utah, Salt Lake City, Utah 84112, United States*

Peter C. Sercel − *Center for Hybrid Organic Inorganic Semiconductors for Energy, Golden, Colorado 80401, United States;* orcid.org/0000-0002-1734-3793

Stephen McGill − *National High Magnetic Field Laboratory, Tallahassee, Florida 32310, United States*

Dmitry Semenov − *National High Magnetic Field Laboratory, Tallahassee, Florida 32310, United States*

Complete contact information is available at: https://pubs.acs.org/10.1021/acs.jpcc.4c08269

Author Contributions

#I.B. and R.B. contributed equally to this work, performing the measurements and analysis. I.B. wrote the bulk of the paper. Z.V.V. supervised the work and contributed to writing the paper. P.S. developed the LL model and contributed to writing the paper.

Notes

The authors declare no competing financial interest.

■ ACKNOWLEDGMENTS

The low-field TRFR setup was supported by the Center for Hybrid Organic Inorganic Semiconductors for Energy (CHOISE) an Energy Frontier Research Center funded by the Office of Basic Energy Sciences, Office of Science within the U.S. Department of Energy through contract number DE-AC36-08G028308. The FAPI film deposition and the TRFR measurements at high magnetic field were supported by the Department of Energy Office of Science, Grant DESC0014579. Experiments were performed at the National High Magnetic Field Lab.

■ REFERENCES

(1) Xing, G.; Mathews, N.; Lim, S. S.; Yantara, N.; Liu, X.; Sabba, D.; Grätzel, M.; Mhaisalkar, S.; Sum, T. C. Low-temperature solution-processed wavelength-tunable perovskites for lasing. *Nat. Mater.* **2014**, *13*, 476.

(2) Odenthal, P.; Talmadge, W.; Gundlach, N.; Wang, R.; Zhang, C.; Sun, D.; Yu, Z.-G.; Vardeny, Z. V.; Li, Y. S. Spin-polarized exciton quantum beating in hybrid organic−inorganic perovskites. *Nat. Phys.* **2017**, *13* (9), 894−899.

(3) Wang, J.; Zhang, C.; Liu, H.; McLaughlin, R.; Zhai, Y.; Vardeny, S. R.; Liu, X.; McGill, S.; Semenov, D.; Guo, H.; et al. Spin-optoelectronic devices based on hybrid organic-inorganic trihalide perovskites. *Nat. Commun.* **2019**, *10*, 129.

(4) Tang, J.; Wang, K. L. Electrical spin injection and transport in semiconductor nanowires: Challenges, progress and perspectives. *Nanoscale* **2015**, *7*, 4325−4337.

(5) Yang, W. S.; Noh, J. H.; Jeon, N. J.; Kim, Y. C.; Ryu, S.; Seo, J.; Seok, S. I. High-performance photovoltaic perovskite layers fabricated through intramolecular exchange. *Science* **2015**, *348*, 1234.

(6) Weber, O. J.; Ghosh, D.; Gaines, S.; Henry, P. F.; Walker, A. B.; Islam, M. S.; Weller, M. T. Phase Behavior and Polymorphism of Formamidinium Lead Iodide. *Chem. Mater.* **2018**, *30* (11), 3768−3778.

(7) Jiang, S.; Luan, Y.; Jang, J. I.; Baikie, T.; Huang, X.; Li, R.; Saouma, F. O.; Wang, Z.; White, T. J.; Fang, J. Phase Transitions of Formamidinium Lead Iodide Perovskite under Pressure. *J. Am. Chem. Soc.* **2018**, *140*, 13952−13957.

(8) Kirstein, E.; Zhukov, E. A.; Yakovlev, D. R.; Kopteva, N. E.; Yalcin, E.; Akimov, I.; Hordiichuk, O.; Dirin, D.; Kovalenko, M.; Bayer, M. Coherent Carrier Spin Dynamics in FAPbBr3 Perovskite Crystals. *J. Phys. Chem. Lett.* **2024**, *15* (10), 2893−2903.

(9) Kirstein, E.; Zhukov, E. A.; Yakovlev, D. R.; Kopteva, N. E.; Harkort, C.; Kudlacik, D.; Hordiichuk, O.; Kovalenko, M. V.; Bayer, M. Coherent Spin Dynamics of Electrons in Two-Dimensional (PEA)2PbI4 Perovskites. *Nano Lett.* **2023**, *23* (1), 205−212.

(10) Kirstein, E.; Yakovlev, D. R.; Glazov, M. M.; Evers, E.; Zhukov, E. A.; Belykh, V. V.; Kopteva, N. E.; Kudlacik, D.; Nazarenko, O.; Dirin, D. N.; et al. Lead-Dominated Hyperfine Interaction Impacting the Carrier Spin Dynamics in Halide Perovskites. *Adv. Mater.* **2022**, *34*, 2105263.

(11) Kopteva, N. E.; Yakovlev, D. R.; Kirstein, E.; Zhukov, E. A.; Kudlacik, D.; Kalitukha, I. V.; Sapega, V. F.; Dirin, D. N.; Kovalenko,

M. V.; Baumann, A.; et al. Weak dispersion of exciton Landè factor with band gap energy in lead halide perovskites: Approximate compensation of the electron and hole dependences. *Small* **2024**, *20*, No. e2300935.
(12) Dai, L.; Deng, Z.; Auras, F.; Goodwin, H.; Zhang, Z.; Walmsley, J. C.; Bristowe, P. D.; Deschler, F.; Greenham, N. C. Slow carrier relaxation in tin-based perovskite nanocrystals. *Nat. Photonics* **2021**, *15*, 696−702.
(13) Huynh, U. N.; Liu, Y.; Chanana, A.; Khanal, D. R.; Sercel, P. C.; Huang, J.; Valy Vardeny, Z. Transient quantum beatings of trions in hybrid organic tri-iodine perovskite single crystal. *Nat. Commun.* **2022**, *13* (1), 1428.
(14) Sheng, C.; Zhang, C.; Zhai, Y.; Mielczarek, K.; Wang, W.; Ma, W.; Zakhidov, A.; Vardeny, Z. V. Exciton versus free carrier photogeneration in organometal trihalide perovskites probed by broadband ultrafast polarization memory dynamics. *Phys. Rev. Lett.* **2015**, *114*, 116601.
(15) Phuong, L. Q.; Yamada, Y.; Nagai, M.; Maruyama, N.; Wakamiya, A.; Kanemitsu, Y. Free carriers versus excitons in CH3NH3PbI3 perovskite thin films at low temperatures: Charge transfer from the orthorhombic phase to the tetragonal phase. *J. Phys. Chem. Lett.* **2016**, *7*, 2316−2321.
(16) Saba, M.; Cadelano, M.; Marongiu, D.; Chen, F.; Sarritzu, V.; Sestu, N.; Figus, C.; Aresti, M.; Piras, R.; Lehmann, A. G.; et al. Correlated electron−hole plasma in organometal perovskites. *Nat. Commun.* **2014**, *5*, 5049.
(17) D'Innocenzo, V.; Grancini, G.; Alcocer, M. J. P.; Kandada, A. R. S.; Stranks, S. D.; Lee, M. M.; Lanzani, G.; Snaith, H. J. Excitons versus free charges in organo-lead tri-halide perovskites. *Nat. Commun.* **2014**, *5*, 3586.
(18) Tong, D. The Quantum Hall Effect, TIFR Infosys Lectures. *arXiv*. **2016**.
(19) Sercel, P. C.; Efros, A. L. Unique signatures of the Rashba effect in the magneto-optical properties of two-dimensional semiconductors. *Phys. Rev. B* **2023**, *107*, 195436.
(20) Yu, Z. G. Effective-mass model and magneto-optical properties in hybrid perovskites. *Sci. Rep.* **2016**, *6*, 28576.
(21) Luttinger, J. M. Quantum theory of cyclotron resonance in semiconductors: General Theory. *Phys. Rev.* **1956**, *102*, 1030−1041.
(22) Löwdin, P.-O. A note on the quantum mechanical perturbation theory. *J. Chem. Phys.* **1951**, *19*, 1396−1401.
(23) Sukmas, W.; Pinsook, U.; Tsuppayakorn-aek, P.; Pakornchote, T.; Sukserm, A.; Bovornratanaraks, T. Organic Molecule Orientations and Rashba−Dresselhaus Effect in α-Formamidinium Lead Iodide. *J. Phys. Chem. C* **2019**, *123*, 16508−16515.

https://doi.org/10.1021/acs.jpcc.4c08269
J. Phys. Chem. C 2025, 129, 5973−5979